Non-muscle myosins 2A and 2B drive changes in cell morphology that occur as myoblasts align and fuse

Nathan T. Swailes*, Melanie Colegrave, Peter J. Knight and Michelle Peckham‡

Institute of Molecular and Cellular Biology, University of Leeds, Leeds, LS2 9JT, UK

*Present address: School of Veterinary and Biomedical Sciences, James Cook University, Townsville, QLD 4811, Australia

‡Author for correspondence (e-mail: m.peckham@leeds.ac.uk)

Accepted 12 June 2006

Journal of Cell Science 119, 3561-3570 Published by The Company of Biologists 2006

doi:10.1242/jcs.03096

Summary

The interaction of non-muscle myosins 2A and 2B with actin may drive changes in cell movement, shape and adhesion. To investigate this, we used cultured myoblasts as a model system. These cells characteristically change shape from triangular to bipolar when they form groups of aligned cells. Antisense oligonucleotide knockdown of non-muscle myosin 2A, but not non-muscle myosin 2B, inhibited this shape change, interfered with cell-cell adhesion, had a minor effect on tail retraction and prevented myoblast fusion. By contrast, non-muscle myosin 2B knockdown markedly inhibited tail retraction, increasing cell length by over 200% by 72 hours compared with controls. In addition it interfered with nuclei redistribution in myotubes. Non-muscle myosin 2C is not involved as western analysis showed that it is not expressed in myoblasts, but only in myotubes. To understand why non-muscle myosins 2A and 2B have such different roles, we analysed their distributions by immuno-electron microscopy, and found that non-muscle myosin 2A was more tightly associated with the plasma membrane than non-muscle myosin 2B. This suggests that non-muscle myosin 2A is more important for bipolar shape formation and adhesion owing to its preferential interaction with membrane-associated actin, whereas the role of non-muscle myosin 2B in retraction prevents over-elongation of myoblasts.

Supplementary material available online at
http://jcs.biologists.org/cgi/content/full/119/17/3561/DC1

Key words: Non-muscle myosin, Myoblasts, Fusion, Antisense, Muscle, Electron microscopy

Introduction

Non-muscle myosin and actin are thought to be important for cell motility, adhesion and cell shape (Cramer, 1999; Maciver, 1996). A good model system for investigating how non-muscle myosins contribute to cell shape is the change in shape of myoblasts that occurs during the early stages of muscle differentiation from a triangular, fibroblast-like to a bipolar morphology (Musa et al., 2003; Wells et al., 1997). Both isolated myoblasts and groups of aligned bipolar cells are dynamic and motile, and myoblasts move at ~1 μm per minute in a similar manner to that of fibroblasts (Peckham et al., 2001). These cell groups form prior to fusion, and adoption of a bipolar morphology probably enables fusion into linear myotubes, with initial fusion predominantly at the ends (Clark et al., 1997; Clark et al., 2002).

The interaction of non-muscle myosins with actin at the plasma membrane in aligned bipolar myoblasts is likely to be responsible for the bipolar shape of these cells. Isolated myoblasts have a triangular shape similar to that of fibroblasts, and non-muscle myosin 2A (NM2A) and NM2B co-localise with the stress-fibre-like actin bundles, cortical actin and the actin meshwork at the base of the lamellipodium (Wells et al., 1997). In aligned groups of bipolar myoblasts, NM2A, NM2B and actin relocalise to the plasma membrane (Wells et al., 1997) and the stress fibre like bundles that contain actin and non-muscle myosin are disassembled. This restricted re-localisation of non-muscle myosins to the membrane is not a fixation artefact, as we found that other myosins (myosin 5 and myosin 9) either did not show this membrane localisation or that they (myosin 1α/Myo1B) were found at the plasma membrane and also had a punctate distribution throughout the cytoplasm (Wells et al., 1997). In addition, drugs that interfere with actin and microtubule organisation affect cell shape and inhibit fusion, demonstrating the importance of both actin and microtubules in fusion (Antin et al., 1981; Holtzer et al., 1975; Siebrands et al., 2004).

The co-localisation of actin and non-muscle myosin in aligned groups of bipolar myoblasts suggests their interaction could be important for cell shape and cell-cell adhesion, but it is not clear whether NM2A and NM2B have similar or distinct roles. In addition, it is possible that the myoblasts express a third, recently identified isoform, non-muscle myosin 2C (NM2C), known to be expressed in skeletal muscle (Golomb et al., 2004). The function of this isoform is unclear, but could contribute to myoblast shape and motility if they express it. We expect the roles of these myosins will be different, as they have been shown to function differently in other systems. Knockout of NM2A results in early embryonic death as the cells fail to adhere (Conti et al., 2004). Knockout of NM2B affects heart and brain development and cardiac cell cytokinesis resulting in death just before or shortly after birth (Bridgman et al., 2001; Takeda et al., 2003; Tullio et al., 1997). NM2C is not as highly expressed in embryonic tissue as NM2A and NM2B (Golomb et al., 2004) and knockdown of NM2C in COS-7 cells had no

effect (Bao et al., 2005), probably because its expression levels are very low in these cells compared with NM2B (NM2A is not expressed). Antisense oligonucleotide knockdown of NM2A in cultured neuroblastoma cells inhibits retraction and adhesion to the substratum, and that of NM2B inhibits neurite outgrowth (Wylie and Chantler, 2001; Wylie and Chantler, 2003; Wylie et al., 1998). Consistent with their different functions, the biochemical kinetics of these three myosins are also distinctly different (Golomb et al., 2004; Kovacs et al., 2003; Rosenfeld et al., 2003; Wang et al., 2003), with NM2A behaving as a normal, relatively fast conventional myosin with a low duty cycle (spends most of its ATPase cycle detached from actin), NM2B behaving as a slow conventional myosin with a higher duty cycle, and NM2C behaving as a slow conventional myosin but with a low duty cycle (Golomb et al., 2004).

Our main goal here was to determine how non-muscle myosins contribute to cell shape, cell adhesion and motility of pre-fusion myoblasts. An antisense oligonucleotide knockdown of NM2A had different effects on cell shape and adhesion compared with NM2B knockdown. To determine why this was the case, we performed a quantitative analysis of NM2A and NM2B distribution at the plasma membrane of bipolar cells by immuno-electron microscopy. Finally, we ruled out a role for NM2C, as we show that this isoform is not expressed in the myoblasts.

Results

Antisense knockdown of NM2A inhibits formation of bipolar cells

Antisense oligonucleotide treatment reduced NM2A mRNA levels by ~40% after 48 hours, and by 60% after 72 hours (Fig. 1). Levels of NM2A mRNA were not affected by sense or scrambled oligonucleotide treatments and remained unchanged in untreated cultures. Actin mRNA was not affected by any treatment. The small cell samples used in our experiments ruled out western analysis. However, in agreement with the RT-PCR results, we also found that the staining intensity of NM2A was reduced in antisense treated cells compared with controls (Fig. 2). The reduction in intensity of staining was reasonably consistent across the culture (Fig. 2).

This reduction in NM2A expression (NM2A knockdown) prevented the formation of elongated bipolar cells in fusing myoblast cultures (Figs 2 and 3). No bipolar cells were found in any of the random fields observed whereas, in control conditions, bipolar cells were found in most fields. Instead, NM2A knockdown resulted in an irregular cell shape and the continued presence of stress-fibre-like bundles that contain residual NM2A (Fig. 3). Interactions between NM2A-knockdown cells were different from that found in controls. In controls, cells have a characteristic bipolar shape, and make tight connections with each other at the end of the cells as shown by the dense actin staining in this region (Fig. 3). By contrast, NM2A-knockdown cells did not appear to make tight connections at their ends (Fig. 3 and Fig. 4A).

Furthermore, NM2A knockdown inhibited fusion, even though cell cultures were dense enough for fusion to occur. We could clearly identify cells that are undergoing differentiation into myotubes in all of the control cultures, but not in the antisense-treated cultures, as shown by their positive staining for skeletal myosin, and the stronger actin staining at the

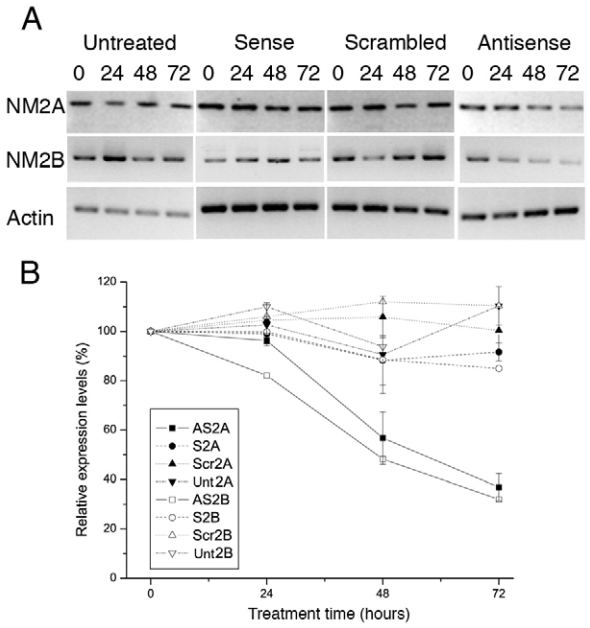

Fig. 1. RT-PCR analysis at 0, 24, 48 and 72 hours of NM2A and NM2B expression levels in knockdown experiments. Data were obtained for untreated, sense, scrambled and antisense cells. (A) Example PCR results are shown for NM2A oligonucleotides and the corresponding β-actin controls, and NM2B oligonucleotides. The data in each row were taken from the same experiment, and the same gel, but the results have been re-organised for display. (B) Time course of RNA levels for NM2A and NM2B in response to oligonucleotide treatment. RNA levels are normalised to actin mRNA in each extract and to the level at the zero time point. n=2 for NM2B; n=3 for NM2A and the error bars (s.e.m.) are shown for NM2A.

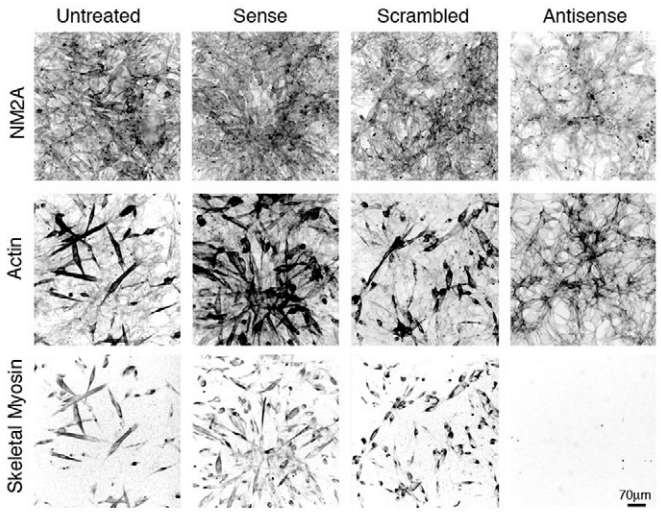

Fig. 2. Effect of NM2A knockdown on myoblast alignment and fusion. The images show intensity-inverted, fluorescent, low-power images of differentiating myoblast cultures left untreated, or treated for 72 hours with sense, scrambled or antisense oligonucleotides for NM2A. The cells were co-stained for NM2A, actin and skeletal myosin. All these images were taken using the same settings, and contrast adjusted equally.

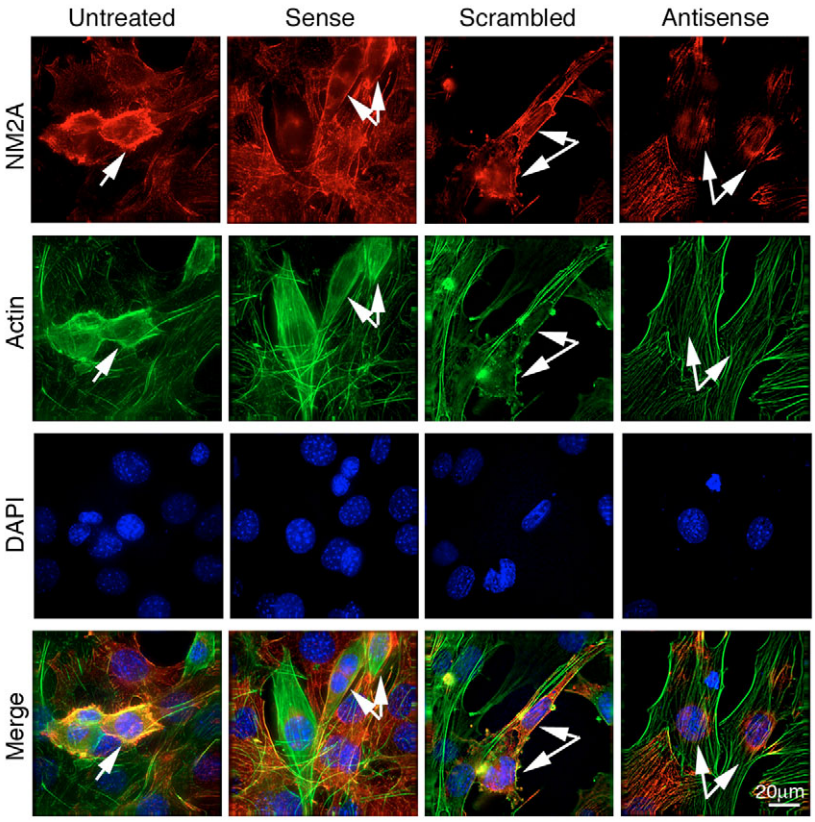

Fig. 3. High power images of differentiating myoblast cultures after 36 hours of treatment, co-stained for NM2A, actin and nuclei. In all the control cultures, cells are present that have a characteristic bipolar shape (arrows), stain strongly for actin compared with non-differentiated cells, and are beginning to align and fuse. By contrast, in NM2A-knockdown cultures, cells have an irregular shape (arrows), and do not form groups of aligned bipolar cells. Bar, 20 μm.

membrane of the bipolar shaped cells compared with undifferentiated cells in the background. By contrast, we did not find any multinucleated myotubes, or cells that expressed skeletal myosin (Fig. 2) in antisense treated cultures.

Cell cultures treated with sense or scrambled oligonucleotides, or left untreated, contained aligned cells with an elongated shape, which had already begun to fuse at 36 hours (Fig. 3). The effects of NM2A-knockdown on fusion could be explained by the failure of the myoblasts to become bipolar in shape and form the groups of aligned cells that are a precursor to fusion. In addition, in order to fuse, the myoblasts must form tight cell-cell adhesions. We noticed that cell-cell contacts in NM2A-knockdown conditions were commonly more tenuous than in control cells (Fig. 4A), and thus the failure of the NM2A-knockdown cells to fuse could also arise from a reduced cell-cell adhesion.

NM2B knockdown affects cell shape and nuclear movement in myotubes

Antisense oligonucleotide treatment reduced NM2B mRNA levels by 50% after 48 hours of treatment, and by 65% after 72 hours (Fig. 1). In agreement with the reduction in mRNA levels, the intensity of NM2B-specific staining in NM2B-knockdown cells was also reduced (Fig. 5).

NM2B knockdown resulted in a strikingly different phenotype to NM2A. First, NM2B knockdown resulted in a striking elongation of cell length (Fig. 4B). However, cells with a bipolar morphology could still be observed, and these cells formed tight connections (Fig. 4B), but elongated connections between cells in aligned groups were evident (Fig. 5B and Fig. 6). In areas of low density, there were fewer groups of aligned cells and many long projections between cells compared with controls (Fig. 5A and Fig. 6).

In regions where cell density was high, we found that, in contrast to NM2A knockdown, NM2B knockdown did not interfere with fusion, as myotubes were formed but the distribution of nuclei in the myotubes was often abnormal (Fig. 7). The ability of these cells to fuse might be expected from the tight cell-cell adhesions present (Fig. 4A) between cells in NM2B-knockdown cultures. Normally, following fusion, the nuclei move apart and are evenly distributed along the

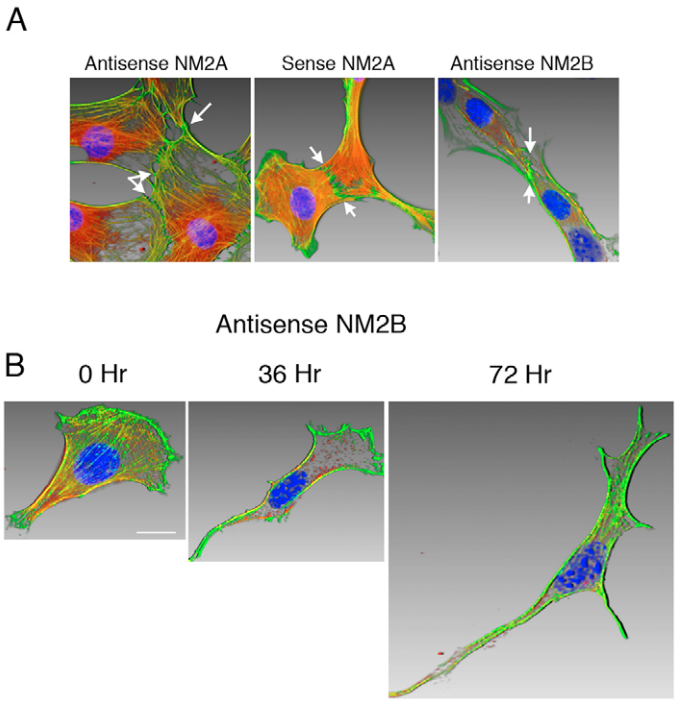

Fig. 4. Blended projection images of NM2A- and NM2B-knockdown cells: effects on cell shape and adhesion. (A) Projection images of NM2A- and NM2B-knockdown and control cells (NM2A-sense treated). The cells have been stained for actin (green), NM2A (for antisense NM2A and sense NM2A) or NM2B (red) and DNA (blue). Sites of interaction between cells are indicated by arrows. (B) A projection image for NM2B-knockdown cells before (0 hours) and after 36 or 72 hours of treatment. The cells have been stained for actin (green), NM2B (red) and DNA (blue). This demonstrates the elongation of the cells following NM2B-knockdown and the change in shape of the lamellipodia. Bar, is 20 μm for all six images.

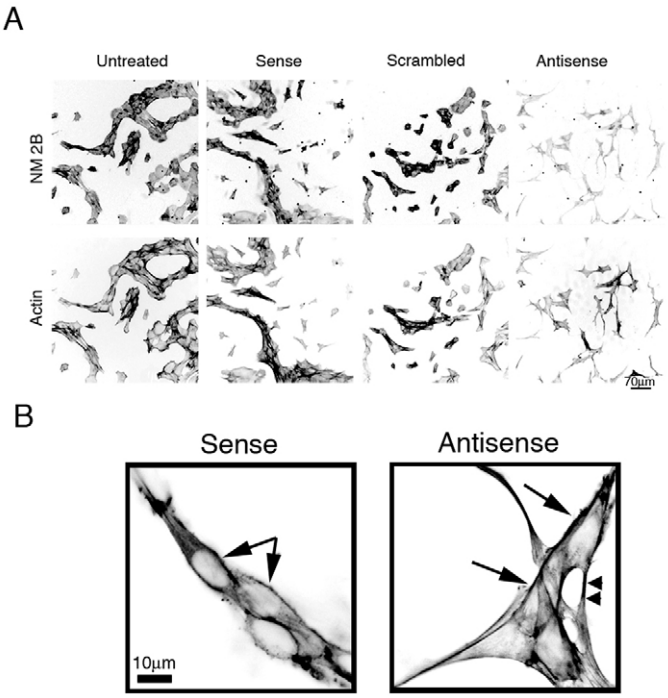

Fig. 5. NM2B-knockdown affects cell shape and alignment. (A) Low power images show intensity-inverted, fluorescent, low-power images of differentiating myoblast cultures left untreated or treated for 72 hours with sense, scrambled or antisense oligonucleotides for NM2B. These images were taken from less dense regions to show the dramatic increase in cell length that results from NM2B treatment, compared with controls. The cells were co-stained for NM2B and actin filaments. Images were taken using the same settings, and contrast adjusted equally for all the images. (B) Intensity-inverted, fluorescent, high-power images of differentiating myoblast cultures stained for actin after 36 hours of treatment with sense or antisense oligonucleotides to compare cell shape and alignment in groups. The arrows show aligned bipolar cells but, in the antisense treatment, elongated connections between cells (arrowheads) are evident.

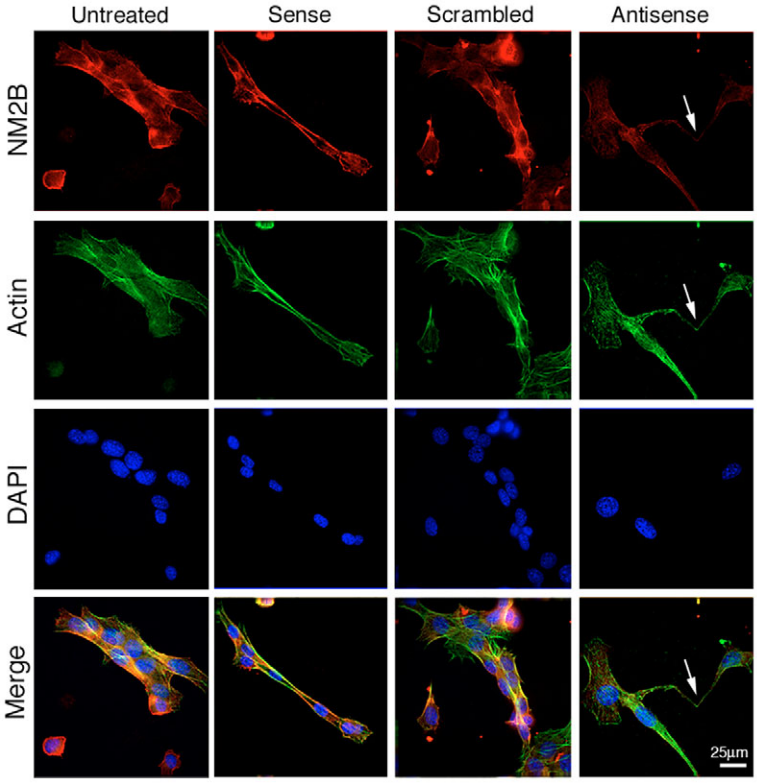

Fig. 6. High power images of myoblasts show NM2B knockdown greatly increases cell length after 36 hours of treatment. Aligned groups containing bipolar cells are present in all of the control conditions but, in NM2B-knockdown cells, the bipolar cells are highly elongated (see arrow) and there is less overlap between them. These images were taken using a ×40 objective lens to enable visualisation of the highly elongated NM2B-knockdown cells.

myotubes (Fig. 8). However, in myotubes formed in NM2B-knockdown cultures, the nuclei were often close together, and had not moved apart. This implicates NM2B also in the movement of nuclei in myotubes following fusion.

The elongation of NM2B-knockdown cells was very striking (Figs 4 and 6). We quantified this by measuring the lengths of cells in the control and NM2B-knockdown cultures from at least two separate experiments. After 72 hours of treatment, we found that the length of NM2B-knockdown cells (198±14 μm, mean±s.e.m., n=54) was significantly longer than control cells (96±5 μm, n=62). There was also a more modest but significant increase in the length of NM2A-knockdown cells (131±6 μm, n=71) that was not apparent from a simple visual inspection of the cells.

Knockdown of NM2B inhibits cytokinesis (Bao et al., 2005). However, our previous work (Morgan et al., 1994) has shown that, in the cells used here under differentiation conditions, cell division decreases such that, after 24 hours, levels of DNA synthesis decrease to 10% of the levels of proliferating cultures, and cease altogether after 48 hours. As we did not start the antisense treatment until 12-24 hours after the switch to differentiation conditions, it is unlikely that any of the effects that we describe here are due to a failure of cytokinesis. Nevertheless, we cannot exclude a small residual effect on cytokinesis that may have resulted in a small reduction in cell density in some experiments.

These analyses show a very different phenotype for NM2A knockdown compared with NM2B knockdown. Knockdown of NM2A interferes with bipolar shape formation, cell-cell adhesion, formation of aligned groups, and fusion but has less effect on cell length. By contrast, knockdown of NM2B results in highly elongated cells that adhere strongly to each other and are able to fuse.

Effects of NM2A or NM2B knockdown on cell locomotion

We suspected that the increased cell length of NM2B-knockdown cells was a result of impaired retraction. We also suspected that the long projections between cells could have arisen from a failure of the cells to detach from each other as they moved apart. Therefore we used time-lapse microscopy of live cells

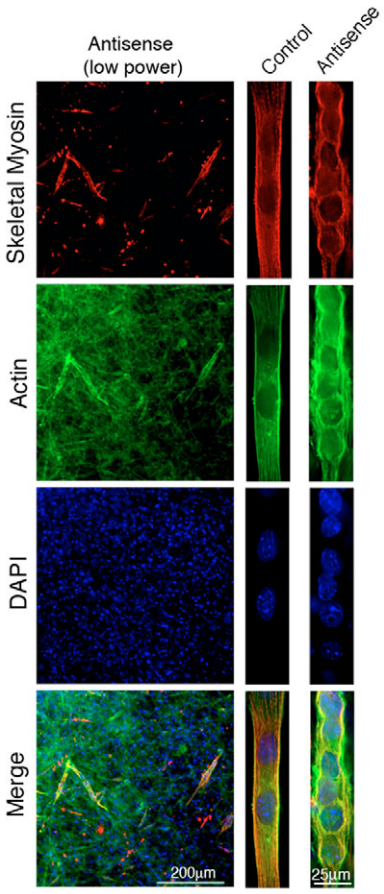

Fig. 7. Immunofluorescent images of NM2B-knockdown cells after 72 hours of treatment in dense cultures shows that cells can still fuse. Cells were co-stained for skeletal myosin (red), actin (green) and DNA (blue). To the left are low-power images that show the presence of myotubes positive for skeletal myosin. To the right are high-power images each showing a myotube formed by NM2B-knockdown cells, compared with a myotube formed in control conditions (sense NM2B-treated). Five nuclei seen in the NM2B-knockdown cells are all very close together, whereas the two nuclei in a similar length of myotube formed by control cells are widely spaced.

to determine whether this was the case, and compared the behaviour of NM2A and NM2B knockdown to control (untreated) cells.

NM2B-knockdown cells were indeed very poor at retraction (Fig. 8 and supplementary material Movie 3) compared with untreated cells (Fig. 8 and supplementary material Movie 1). We commonly observed that the tail never actively retracted, but as the cell body moved forward, the tail became more and more elongated until it broke. The average length of time over which the tails persisted was 140±20 minutes (mean±s.e.m.; n=13) compared with 30±5 minutes (n=14) for untreated cells. In addition, we also observed that, as cells attempted to move apart from each other, they often failed to separate, resulting in elongation and eventually cell breakage (Fig. 8). This failure to retract can account for the increase in cell length that we measured for NM2B-knockdown cells.

NM2A knockdown also had an effect on retraction (Fig. 8 and supplementary material Movie 2) in that a short but obvious tail persisted for a similar length of time (125±20 minutes, n=14) as observed for NM2B. In contrast to NM2B-

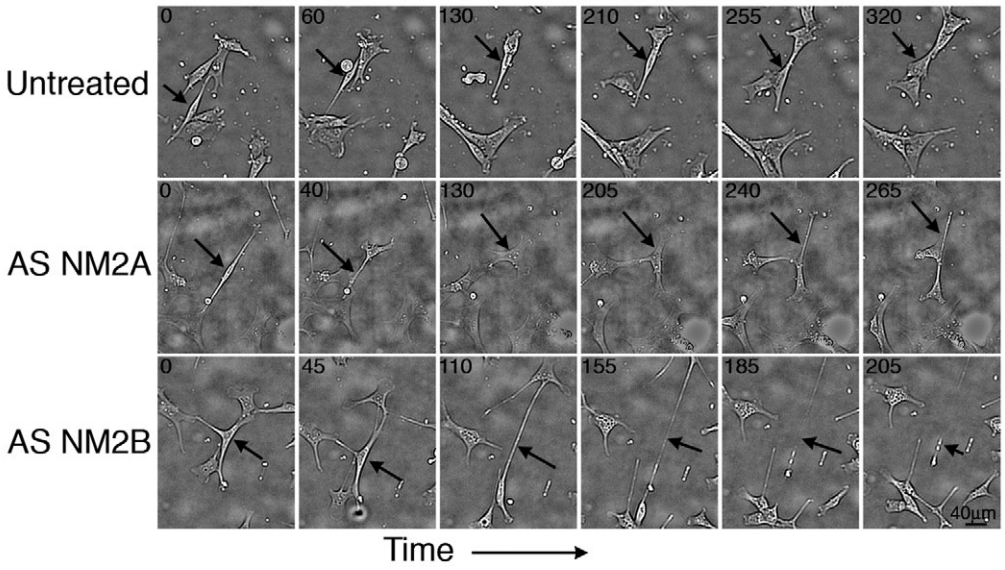

Fig. 8. Still images from a time-lapse experiment for NM2A- or NM2B-knockdown. Three sets of montages are shown, one each for untreated, NM2A- or NM2B-knockdown cells, from a single time-lapse DIC imaging experiment. The cells were left untreated or treated with antisense oligonucleotides for 24 hours before the start of filming, and filmed for the next 18 hours immediately after adding additional oligonucleotides. The numbers shown in the corner of each frame are the time elapsed since the first frame (time=0) in minutes (frame interval was 5 minutes). The arrows for the untreated cells show the progress of a single cell as it forms part of an aligned group of bipolar cells. The arrows for the NM2A-knockdown experiment show a single cell that tends to have a longer tail than controls but is able to retract. The arrows for the NM2B-knockdown experiment show a cell that becomes highly extended as it interacts with, and fails to detach from, other cells in the culture, and eventually its tail breaks (at t=185 minutes). See also supplementary material Movies 1-3.

knockdown cells, however, the lengths of the tails in NM2A-knockdown cells was shorter and cell breakage was less common. This effect on retraction could account for the increased length of antisense NM2A-knockdown cells that we measured at 72 hours. Although a noticeable tail was found to persist over a similar time interval for NM2A and NM2B, measurements from fixed cells, and from the live cell imaging showed that the lengths of the NM2A-knockdown-treated cells were shorter than those for NM2B-knockdown cells.

Additionally, we found that the area of the lamellipodium for antisense NM2B-treated cells in the live cell images was reduced. Quantifying this by measuring the area of the cell in front of the nucleus, which is mainly made up of the lamellipodium, we found that the area of the lamellipodia in NM2B-knockdown cells (635±47 μm^2, mean±s.e.m., n=42) was reduced by about 50% compared with antisense NM2A (1378±87 μm^2, n=49) or untreated (1561±130 μm^2, n=63) cells.

Although NM2B- and NM2A-knockdown cells were clearly less good at retracting compared with untreated cells, this only had a small effect on the overall cell speed. Thus, the failure of the tail to retract does not appear to oppose the forward motion of the cells. The speed of NM2B-knockdown cells (0.39±0.15 $\mu m\ min^{-1}$, mean±s.d., n=27), was only slightly reduced compared with that for untreated cells (0.51±0.37 $\mu m\ min^{-1}$, n=30) and NM2A-knockdown cells (0.55±0.27 $\mu m\ min^{-1}$, n=30).

Myoblasts do not express NM2C

Given the marked effects of NM2A and NM2B knockdown on cell morphology and differentiation, we checked whether the recently discovered non-muscle myosin 2C (NM2C) (Golomb et al., 2004) was also expressed in the myoblasts. We used both RT-PCR and western analysis to investigate whether the myoblasts express this isoform in addition to NM2A and NM2B. We did not detect a transcript for this myosin by RT-PCR using specific primers in myoblasts, although specific primers for NM2A and NM2B were both positive (data not shown). Furthermore, we did not detect expression of this isoform in myoblasts (Fig. 9) by western analysis, although we could detect its expression in differentiated myotubes. By contrast, we could easily detect the expression of NM2A in both myoblasts and myotubes (Fig. 9). Thus NM2C has no role in the early stages of myoblast differentiation.

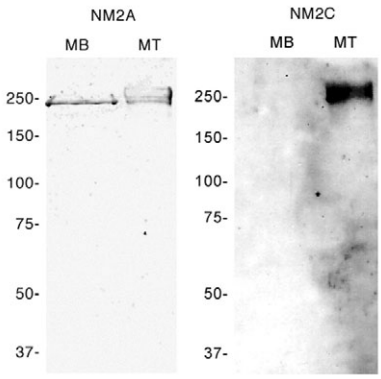

Fig. 9. Western analysis of NM2A and NM2C expression in myoblasts (MB) and 3 day myotubes (MT). Western analysis shows a positive band of the correct size for NM2A in myoblasts and myotubes. By contrast, despite using a longer exposure time (and hence higher background), a positive band of the correct size for NM2C was only observed in myotubes and not in myoblasts. Protein loading in each of the lanes was the same.

Distribution of NM2A and NM2B within aligned cells

To understand the different contributions of NM2A or NM2B to bipolar cell shape and adhesion, we analysed their distribution in aligned bipolar myoblasts by immuno-electron microscopy. The majority of actin and both NM2A and NM2B are localised at the plasma membrane in aligned cells (Wells et al., 1997) as shown here for aligned cells co-stained for actin and NM2B (Fig. 10A). Therefore we expected that the immuno-electron microscopy would also show a narrow distribution of non-muscle myosins at the plasma membrane and very little staining in the middle of the cell. However, we anticipated that we might be able to discern small changes in the relative distributions of these two myosin isoforms, as our original confocal images hinted that the staining for NM2B might be slightly broader than that for NM2A in aligned cells (Wells et al., 1997). The cells used in the immuno-EM experiments here were fixed and stained in the same way as for fluorescence microscopy, but using an immunogold-labelled secondary antibody instead of a fluorescent one, and therefore we expect that penetration of the gold-labelled antibodies should be the same as that for immunofluorescence.

After processing and sectioning the cells for electron microscopy, we found that the morphology of fixed, permeabilised and antibody-labelled cells was well preserved when compared with control (non-permeabilised) cells in electron micrographs (Fig. 10B). The cells observed in EM sections had formed aligned groups that appeared identical to those that had been fixed, stained and viewed in the light microscope. In these groups, cells displayed the typical elongated shape of aligning cells and were easily identified. They were ~45 μm in length, 8-10 μm wide and had a ventro-dorsal thickness of 2.7–4.0 μm (calculated from the number of TEM sections between the first ventral and last dorsal section, which was 45 on average).

We found that, in agreement with our earlier confocal images, the majority of NM2A and NM2B were found close to the plasma membrane (Fig. 10C-E). However, NM2A had a tighter distribution with respect to the plasma membrane compared with NM2B. Seventy-four percent of NM2A lay within 0.5 μm of the plasma membrane compared with only 57% of NM2B. The distribution of particles was similar in ventral, middle and dorsal sections, and all along the length of the cells, from a chi-square analysis for NM2A. Thus all the data, except that from the ends of the cells, were pooled and the distributions for each of the three cells labelled with NM2A were compared (Fig. 10C). The distributions of NM2A in each cell were similar (Fig. 10C), and these data were again pooled for the final comparison of the distributions of NM2A and NM2B (Fig. 10E). A similar analysis for NM2B showed that the distributions of NM2B in three separate cells were similar (Fig. 10D) and this data was again pooled to compare the distributions of NM2A and NM2B (Fig. 10E).

Our finding that the overall distribution of NM2B was broader than that for NM2A (Fig. 10E) is unlikely to be due to a difference in labelling densities, as the labelling density

for NM2A and NM2B was similar, considering the varying efficiencies of the two primary antibodies. The number of particles counted per 2 μm^2 quadrat in all sections from the 3 cells was 43±7 particles (mean±s.e.m., n=255 sections) for NM2A and 39±5 particles (n=237) for NM2B-labelled cells. Furthermore, there was no evidence that the penetration of the two different antibodies was different, as we found that the minimum distance of the gold particles away from the plasma membrane was the same for NM2A and NM2B (5 nm), and the maximum distance was actually greater for NM2A (1939 nm) compared with NM2B (1521 nm). However, the mean distance away from the plasma membrane was significantly higher for NM2B than for NM2A (318±3 nm, n=10,966, for NM2A; compared with 442±3 nm, n=9,180 for NM2B, mean±s.e.m.).

This overall difference in distribution of NM2A and NM2B could explain the different effects of NM2A and NM2B-knockdown we observed. NM2A distribution closely matches the 0.5 μm-thick subplasmalemmal actin band that we described previously for the aligned myoblasts (Swailes et al., 2004), and is more likely to interact with actin filaments close to the membrane, influencing cell shape and adhesion. Although a significant proportion of NM2B also overlaps this band of actin, its broader distribution suggests it is more important in interacting with actin filaments further inside the cell, explaining the lack of effects on adhesion and bipolar shape that we observed for NM2B knockdown.

Discussion

Overall, our results show that the interactions between non-muscle myosins and actin are crucial for the morphology of the myoblasts, and this is also likely to be the case in fibroblasts,

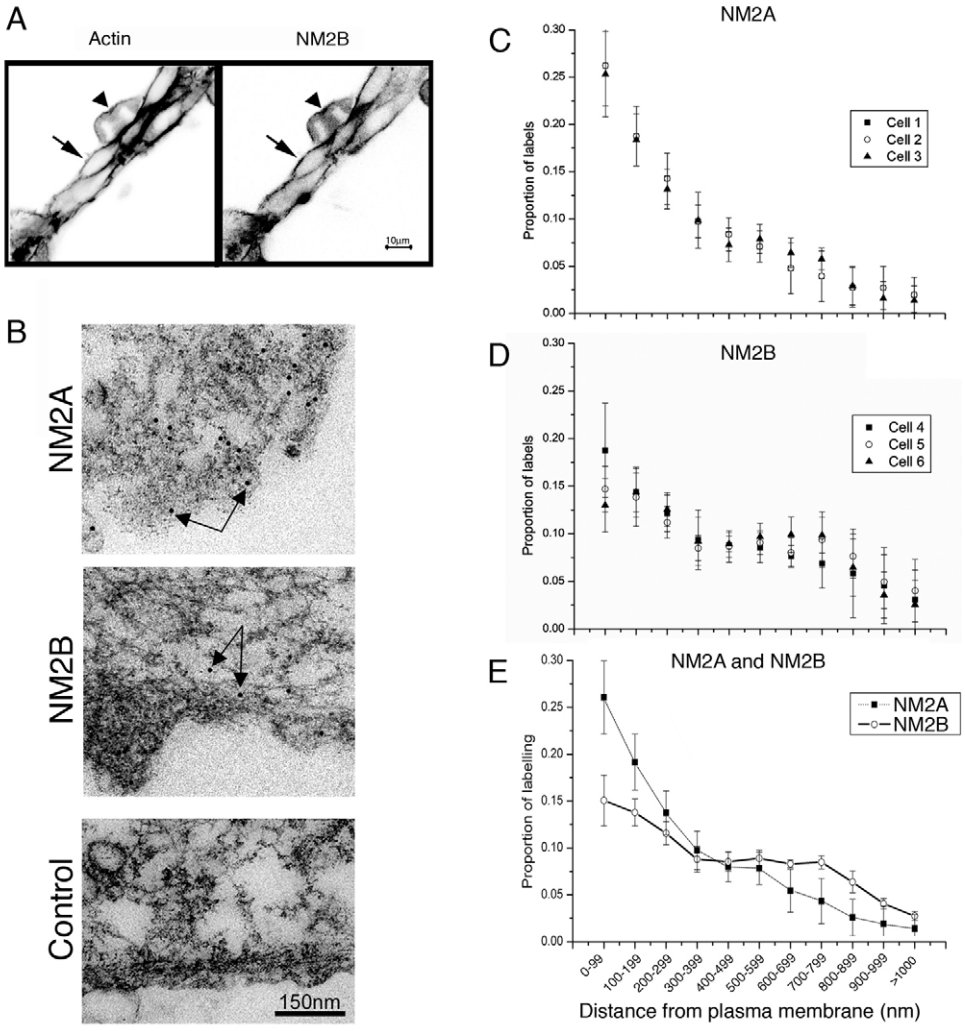

Fig. 10. Distributions of NM2A and NM2B by immuno-electron microscopy. (A) A single confocal slice from a group of aligned bipolar cells co-immunostained for NM2B, actin and DNA (DAPI). The majority of actin and non-muscle myosin (NM2B) is found at the plasma membrane (arrow). The arrowhead denotes a cell that is in the final stages of cell-division, that remains associated with the group of aligned cells. The staining pattern for NM2A is similar, and the staining shown here is similar to that reported earlier (Wells et al., 1997). (B) Representative electron micrographs of sections near the ventral surface of aligned myoblasts labelled with a primary antibody raised against NM2A, or a primary antibody raised against NM2B. The gold particles can be seen clearly, and only on the cytoplasmic side of the plasma membrane. For comparison, a control section is shown in which the primary antibody was omitted. No gold particles are observed in the control cells. (C) Distribution of gold particles for NM2A in three aligned cells, with respect to the plasma membrane. The mean±s.d. for each cell is shown, where n=10, and represents the number of different sampling positions, at 5 μm intervals from one end of the cell to the other along each of the cells. Nine sections (three dorsal, three middle and three ventral) were averaged together for each sampling position after the proportion of gold particles within each 100 nm bin was calculated. In total, the distance of 10,966 particles from the plasma membrane was measured and used in this analysis. Labels for the x-axis are as shown for E. (D) Distribution of gold particles for NM2B with respect to the plasma membrane in three aligned cells. The mean±s.d. is shown as for NM2A in C. In total, the distance of 9180 particles from the plasma membrane was measured and used in this analysis. Labels for the x-axis are as shown for E. (E) A direct comparison of the distributions of NM2A (mean for three cells shown in C) and NM2B (mean for three cells shown in D) gold labelled particles in the six aligned cells. As no significant differences (by chi-square test) were observed in the distribution of particles at each of 5 μm sampling positions along the cells, or between cells, the data were pooled into a single figure for the three cells for each myosin isoform. For NM2A and NM2B, the mean±s.d. is shown, where n=3 (number of cells).

which have a similar shape and actin organisation. We determined that, in myoblasts, only NM2A and NM2B are involved, as the myoblasts do not express NM2C. NM2A and NM2B have different, but overlapping, distributions within aligned myoblasts. Three-quarters of NM2A was found within 0.5 μm of the plasma membrane, whereas only slightly more than half of NM2B was found within this zone. These results suggested that NM2A is more important than NM2B in interacting with the population of actin filaments found close to the plasma membrane. We tested the potential role of NM2A in myoblast alignment and fusion and found that knockdown of NM2A prevented aligned groups of myoblasts from forming, and consequently inhibited fusion by apparently weakening cell-cell attachment and bipolar shape formation. By contrast, knockdown of NM2B resulted in bipolar shaped cells that were much more elongated than normal, were poor at retraction, but were still able adhere to each other and fuse. Thus these myosins have separate functions in formation of aligned bipolar myoblasts and cannot entirely compensate for one another.

Knockdown of NM2A and NM2B suggest that NM2A plays the greater role in generating the bipolar shape of aligned myoblasts, and in cell-cell adhesion, whereas NM2B has the greater role in cell retraction. Cell-cell adhesion, and bipolar shape formation are both likely to arise from an interaction of NM2A with the cortical actin (or subplasmalemmal actin sheet) that is in close proximity to the plasma membrane. This interaction would transmit tension to the plasma membrane, and to adhering cells, via transmembrane adhesion molecules such as cadherins, integrins or dystrophins. This type of role is consistent with the tight overlap between NM2A and the subplasmalemmal actin sheet. Non-muscle myosin was implicated in 'coralling' proteins involved in adhesion to sites of cell-cell contact (Shewan et al., 2005). From the results presented here, it is likely that NM2A is the non-muscle myosin responsible for this. It is also possible that its 'fast' kinetics enable rapid tension responses to be switched on or off, enabling fast responses to external cues or cell signalling events.

Our observation that NM2A-knockdown interferes with cell-cell adhesion is also consistent with the earlier demonstration that knockout of NM2A in mice results in the loss of cell-cell adhesion and failure of the embryo to develop beyond day E7.5 (Conti et al., 2004). Intriguingly, we found that NM2B, rather than NM2A, played the major role in retraction and that NM2A knockdown did not affect cell-substrate adhesion as previously reported for neuroblastoma cells, using a similar knockdown approach (Wylie and Chantler, 2003; Wylie et al., 1998). In neuroblastoma cells, NM2A, and not NM2B, is the retraction motor, and NM2B-knockdown decreases cell length whereas, in myoblasts, NM2B knockdown increases it. However, it may be difficult to compare directly our results with those from neuroblastoma cells for two reasons. First, the experiments in neuroblastoma cells looked at retraction in response to thrombin or lyphosphatidate, which are likely to result in a decreased basal cytoplasmic tension, whereas here we are looking at the retraction of the tail of motile cells as they move forward, as a result of contractile activity. Second, the absolute levels of NM2A and NM2B in myoblasts may be different to those in neuroblastoma cells.

The lack of effect of NM2B knockdown on formation of a bipolar shape could be explained by the broader distribution of this myosin in the vicinity of the plasma membrane, such that it is less abundant in regions close to the plasma membrane, but more abundant deeper into the cell compared with NM2A. Therefore we would expect NM2B to be less important in interacting with the actin cytoskeleton close to the plasma membrane, and thus would not play such an important role in cell shape and cell-cell adhesion. Not surprisingly, myoblasts were still able to fuse into myotubes when NM2B was knocked down, as the continued presence of NM2A will enable the tight cell-cell adhesion required for fusion to occur. However, NM2B did interfere with retraction and cell-cell detachment resulting in cell elongation. This decrease in cell retraction is likely to be important when cells interact to form aligned groups of myoblasts in vitro, as time-lapse images of fusing myoblasts have shown that there are considerable changes in cell morphology, in which extension and retraction are both evident up to the point of fusion (Musa et al., 2003).

The effect of NM2B knockdown on retraction in myoblasts that we have observed here is consistent with that reported for fibroblasts derived from the NM2B-knockout mouse (Lo et al., 2004). NM2B has also been implicated in local tension generation in growth cones, required for the cells to turn (Turney and Bridgman, 2005). Our results also show that there is a link between NM2B activity and retraction-induced protrusion. It is well known that spontaneous or microneedle-induced tail retraction of fibroblasts results in enhanced protrusive activity at the leading edge of the cell shortly afterwards (Chen, 1979; Dunn, 1980), that tail retraction involves a phase of active contraction (Chen, 1981), and that there is a correlation between retraction and protrusion (Dunn and Zicha, 1995). We have also shown previously that actomyosin contraction could influence protrusion (Peckham et al., 2001). Our finding that NM2B antisense treatment not only reduced retraction, but also reduced the size of the lamellipodium, suggests that NM2B is the myosin isoform responsible for the link between retraction and protrusion.

Surprisingly, although we found that NM2B knockdown did not interfere with fusion, the nuclei in the myotubes formed commonly remained in close contact and did not disperse. In mature muscle fibres, nuclei are known to be spatially dispersed along the fibre (Bruusgaard et al., 2003; Bruusgaard et al., 2006), and it was reported that microtubules are involved in this spatial dispersion. A role for non-muscle myosin and the actin cytoskeleton has not been reported before and merits further examination. NM2B knockout does not interfere with skeletal muscle fibre formation in vivo (Tullio et al., 1997), but the spatial arrangement of nuclei in the muscle has not been reported. Some models of myofibrillogenesis suggest that skeletal myosin replaces non-muscle myosin in developing sarcomeres (Dabiri et al., 1997; Sanger et al., 2002). However, if this is the case, the non-muscle myosin involved is unlikely to be NM2B, as we could still observe muscle sarcomeres in the NM2B knockdown myotubes.

Taken together, our results suggest that, in myoblasts, there is a critical balancing act between NM2B and NM2A that controls the relative extents to which the cells can elongate or retract in order to form the elongated cell shape typical of aligned groups. NM2A plays an additional role in enabling the aligned cells to adhere to each other. The adoption of a bipolar shape is characteristic of pre-fusion myoblasts. The different

contributions of NM2A and NM2B to this shape change in myoblasts further suggests that, in other cell types, the location and expression levels of different non-muscle myosins are likely to play a major role in cell shape and cell-cell adhesion.

Materials and Methods

Growth and differentiation of H-2k^b-tsA58 myogenic cells

Mouse H-2k^b-tsA58 myoblasts were used, cultured as described previously (Morgan et al., 1994; Swailes et al., 2004; Wells et al., 1997). Briefly, myoblasts were proliferated at 33°C in the presence of IFN-γ in standard growth medium (DMEM, 20% FCS, 1% CEE, 1% penicillin/streptomycin) and differentiated into myotubes at 37°C in the absence of IFN-γ in differentiation medium (DMEM, 5% FCS, 2% CEE, 1% penicillin/streptomycin). For immunofluorescence and immuno-electron microscopy, cells were cultured on washed glass coverslips or Aclar coverslips respectively, which were pre-coated with rat-tail collagen. For western analysis, cells were grown in flasks, and protein samples (equally loaded) were run on 7.5% SDS-PAGE gels, transferred to nitrocellulose and incubated with antibodies to NM2C (rabbit polyclonal, a gift from Martin Rumsby, University of York, UK) or NM2A (a gift from R. Adelstein, NIH, Bethesda, MD), washed, and then incubated with HRP-conjugated anti-rabbit secondary antibodies. Positive bands detected by ECL (Pierce).

Treatment of cells with oligonucleotides

Mouse H-2k^b-tsA58 myogenic cells were proliferated for 1-2 days on glass coverslips coated with matrigel, or (for the NM2B treatments at high cell density) with 1% gelatin, as described above until they had reached a suitable density for fusion. The cells were then cultured in differentiating medium at 37°C for 10-12 hours, before starting treatment with the oligonucleotides. The oligonucleotides used for the antisense NM2A experiments in this study were the same as those described previously (Wylie and Chantler, 2001), named AQ3 (antisense), AQ5 (sense) and AQ3R (scrambled). The oligonucleotides used for NM2B were antisense (AS2B) GGATTCCAGAATTGGATTTGC; Sense (S2B) (GCA AATC-CAATTCTGGAATCC) and scrambled (SCR2B) GGCTACGATGACAGGTA-TTTT. These oligonucleotides are similar to those previously published for NM2B in neuronal cells (Wylie et al., 1998) but are based on the non-neuronal isoform sequence (accession number: NM175260), base pair changes are underlined. An initial test showed that even though there are only two base-pair differences, the neuronal isoform specific oligonucleotides were not effective in reducing NM2B expression levels in myoblasts (N.T.S., P.J.K. and M.P., unpublished data).

To treat the cells with oligonucleotides, the cells were washed in serum-free medium (50:50 Nutrient Mixture F-12 Ham and MCDB201; Sigma), and transferred into fresh filtered serum-free media containing 50 μM of oligonucleotide (HPLC purified, Sigma-Genosys). Subsequently at 12 hour intervals, the medium was supplemented with additional oligonucleotides (25 μM) to replenish degraded oligonucleotides. Cells were treated with antisense (AQ3 or AS2B), sense (AQ5 or S2B) or scrambled (AQ3R, or SCR2B) oligonucleotides every 12 hours for a total of 72 hours (Wylie and Chantler, 2001) or left untreated.

RT-PCR of oligonucleotide treated cells

RNA expression levels of NM2A, NM2B and actin were analysed by RT-PCR. At each time point (0, 24, 48 and 72 hours), total RNA was isolated from cells using RNAzol (Biogenesis) and used to make cDNA, which was subsequently used in a PCR reaction. The forward primers were the same as described previously (Wylie and Chantler, 2001). The reverse primers used were AQ3 or AS2B for NM2A and NM2B, respectively. Actin primers to mouse β-actin were used as a control as previously described (Wylie et al., 1998). The actin primers yielded an amplification product of 514 bp, NM2A primers an amplification product of 680 bp, and NM2B primers an amplification product of 622 bp. The PCR bands were examined by agarose gel electrophoresis, captured digitally using the Gel-Doc system (Biorad), and the band intensities at each time point were quantified using Scion Image software (Scion Corporation). The intensities were normalised by dividing the intensity for each non-muscle myosin band by the intensity of the corresponding actin bands for each sample to take account of potential differences in the amount of cDNA template obtained. The data for antisense, sense, scrambled and untreated samples were normalised to the zero time point.

Immunofluorescence and deconvolution microscopy of oligonucleotide treated cells

In addition to RT-PCR analysis, coverslips were taken from cultures after 36 and 72 hours of oligonucleotide treatment. These coverslips were fixed and stained for either NM2A or NM2B using the same primary antibodies as for immuno-electron microscopy. Actin was stained using Alexa phalloidin 488, and secondary antibodies used were anti-rabbit Alexa 568 (Molecular Probes). Nuclei were labelled with DAPI (Molecular Probes). In some cases the coverslips were additionally stained for skeletal myosin, as a marker of myofibrillogenesis, using the primary antibody A1025 (Cho et al., 1994). Images of fixed and stained cells were captured using a Deltavision deconvolution microscope using either a ×10 or ×60 objective. The same exposure times were used for non-muscle myosin for each treatment. Images were imported into Photoshop (Adobe) and the contrast adjusted by the same amount. Projections were made using three sections from a Z-stack of deconvolved images in Imaris. To measure cell length, images of cells taken using the ×10 objective were imported into Lucida (Kinetic Imaging Software).

Time-lapse imaging

Cells on coverslips in a 4-well Petri dish were treated with oligonucleotides as described above, or left untreated. After 24 hours, the cells were again treated with oligonucleotides and then placed on the motorised stage of an Olympus microscope, enclosed by an incubator at 37°C, 5% CO_2. Cells were imaged using DIC optics, and a ×10 objective. Images were taken once every 10 minutes for 18 hours, from nine different fields: three from untreated cells, three from antisense NM2A-treated cells and three from antisense NM2B-treated cells. Images were captured using multi-point visiting, driven by image capture software (Softworx, Deltavision, USA). The resulting image sequences were imported into a tracking program (Kinetic Imaging) to measure cell speeds and dimensions. To measure cell speed, cells were tracked in sequential frames by clicking on the position of the nucleus. The areas of the lamellipodia were measured using Scion Image Software. Standard time-lapse imaging was also performed on cultures of fusing myoblasts in culture flasks by phase-contrast time-lapse microscopy, at 37°C.

Immunogold labelling of aligned cells and serial sectioning

Cells were lightly fixed using 2% paraformaldehyde for 30 minutes, permeabilised using 0.1 mg/ml saponin in MOPS buffered Ringer (127 mM NaCl, 4 mM KCl, 1 mM $MgCl_2$, 1 mM $CaCl_2$, 5 mM glucose, 10 mM MOPS) and rinsed gently in PBS prior to treatment with primary antibodies. The primary antibodies used in this study were rabbit polyclonals: anti-NM2A and anti-NM2B (gifts from R. Adelstein, NIH). The cells were incubated with the primary antibody for 60-120 minutes, washed and then incubated with the secondary 10 nm gold-conjugated goat anti-rabbit antibody (BBInternational) using a similar protocol to that used for immunofluorescence. As a control for monitoring non-specific labelling, cells were treated in the same way but the primary antibody was omitted. Some coverslips were also left unpermeabilised to monitor the effects of saponin treatment.

Following antibody treatment, cells on coverslips were post-fixed in MOPS buffered Ringer containing 3% glutaraldehyde for 30 minutes, thoroughly rinsed in MOPS buffered Ringer to remove unbound glutaraldehyde, post-fixed on ice for 10 minutes in 1% osmium tetroxide (made up from a 2% stock in 10 mM $MgCl_2$ and 100 mM K-phosphate, pH 6.1), washed in MOPS buffered Ringer, stained in 2% uranyl acetate for 15 minutes at 4°C and subsequently washed with distilled water. The cells were then dehydrated using an ethanol gradient and embedded as described previously (Swailes et al., 2004). After removal of the aclar coverslips, serial sections, 60-90 nm thick, were then taken through the cells, from the bottom to the top and sections stained as described (Swailes et al., 2004). We could not estimate exactly how close to the bottom of the cell the first sections we analysed were cut. The aligned cells are 'rugby ball' shaped, and the sections have low contrast, the most dorsal or ventral regions difficult to identify. In addition, it would be difficult to distinguish whether gold particles in sections close to either the ventral (or dorsal) surfaces of the cell were closest to the ventral (or dorsal membranes), or to the lateral membranes [i.e. we would need to be at least ten 60-90 nm sections below the top (or bottom) surface before a point 700 nm from the lateral edge was further from the top (or bottom) than the side]. By avoiding these sections, we avoid this problem.

EM quantitation

TEM sections were observed using a JEOL 1200EX operated at 80 kV. To observe gold particles, areas of selected regions in aligned cells were photographed at a nominal magnification of 12,000× or 15,000×. Negatives were scanned at 20 μm pixel size and the magnification calibrated using Fourier transforms of the 14.4 nm paramyosin repeat. These digitised images were viewed in Photoshop. All subsequent measurements were made using these images. Gold particles were easily identified as smoothly circular electron dense dots, measuring 10 nm in diameter.

The numbers of gold-labelled particles and their distance from the lateral cell plasma membrane were measured using a quadrat-based sampling protocol. A 1 × 2 μm rectangle was superimposed on the micrograph, such that one short side lay superimposed on and roughly parallel to the plasma membrane, while the longer edge extended into the cell body perpendicular to the membrane. The number of gold particles within the rectangle was recorded, and the distance of each particle from the plasma membrane was measured using a line drawn from the centre of the gold dot to transect the plasma membrane at 90°. This sampling was repeated by placing the rectangle on the micrograph at 5 μm intervals from one end of the cell to the other, and for three ventral, three middle and three dorsal sections (each set of three encompassing 0.75 μm of cell thickness). In order to prevent any form of bias sampling, measurements were made 'blind' (without knowing which cell or section the image came from, without knowing the orientation of the image relative to the cell, and without knowing the orientation of the cell). In total, 10,966 particles were counted in three separate NM2A-labelled cells and 9180 particles in NM2B-

labelled cells, and the distance of every particle from the plasma membrane was measured.

We thank Professor Peter Chantler (RVC, London) for an initial supply of antisense NM2A oligonucleotides for preliminary experiments, Hanny Musa for assistance in setting up the PCR, the Anatomical Society (Great Britain) for funding a studentship to N.T.S., and BBSRC and the Wellcome Trust for funding the imaging equipment used in this work.

References

Antin, P. B., Forry-Schaudies, S., Friedman, T. M., Tapscott, S. J. and Holtzer, H. (1981). Taxol induces postmitotic myoblasts to assemble interdigitating microtubule-myosin arrays that exclude actin filaments. *J. Cell Biol.* **90**, 300-308.

Bao, J., Jana, S. S. and Adelstein, R. S. (2005). Vertebrate nonmuscle myosin II isoforms rescue small interfering RNA-induced defects in COS-7 cell cytokinesis. *J. Biol. Chem.* **280**, 19594-19599.

Bridgman, P. C., Dave, S., Asnes, C. F., Tullio, A. N. and Adelstein, R. S. (2001). Myosin IIB is required for growth cone motility. *J. Neurosci.* **21**, 6159-6169.

Bruusgaard, J. C., Liestol, K., Ekmark, M., Kollstad, K. and Gundersen, K. (2003). Number and spatial distribution of nuclei in the muscle fibres of normal mice studied in vivo. *J. Physiol.* **551**, 467-478.

Bruusgaard, J. C., Liestol, K. and Gundersen, K. (2006). Distribution of myonuclei and microtubules in live muscle fibres of young, middle-aged and old mice. *J. Appl. Physiol.* **100**, 2024-2030.

Chen, W. T. (1979). Induction of spreading during fibroblast movement. *J. Cell Biol.* **81**, 684-691.

Chen, W. T. (1981). Mechanism of retraction of the trailing edge during fibroblast movement. *J. Cell Biol.* **90**, 187-200.

Cho, M., Hughes, S. M., Karsch-Mizrachi, I., Travis, M., Leinwand, L. A. and Blau, H. M. (1994). Fast myosin heavy chains expressed in secondary mammalian muscle fibers at the time of their inception. *J. Cell Sci.* **107**, 2361-2371.

Clark, P., Coles, D. and Peckham, M. (1997). Preferential adhesion to and survival on patterned laminin organizes myogenesis in vitro. *Exp. Cell Res.* **230**, 275-283.

Clark, P., Dunn, G. A., Knibbs, A. and Peckham, M. (2002). Alignment of myoblasts on ultrafine gratings inhibits fusion in vitro. *Int. J. Biochem. Cell Biol.* **34**, 816-825.

Conti, M. A., Even-Ram, S., Liu, C., Yamada, K. M. and Adelstein, R. S. (2004). Defects in cell adhesion and the visceral endoderm following ablation of nonmuscle myosin heavy chain II-A in mice. *J. Biol. Chem.* **279**, 41263-41266.

Cramer, L. P. (1999). Organization and polarity of actin filament networks in cells: implications for the mechanism of myosin-based cell motility. *Biochem. Soc. Symp.* **65**, 173-205.

Dabiri, G. A., Turnacioglu, K. K., Sanger, J. M. and Sanger, J. W. (1997). Myofibrillogenesis visualized in living embryonic cardiomyocytes. *Proc. Natl. Acad. Sci. USA* **94**, 9493-9498.

Dunn, G. A. (1980). Mechanisms of fibroblast locomotion. In *Cell Adhesion and Motility, 3rd Symposium of the British Society for Cell Biology* (ed. A. S. G. Curtis and J. D. Pitts), pp. 409-423. Cambridge: Cambridge University Press.

Dunn, G. A. and Zicha, D. (1995). Dynamics of fibroblast spreading. *J. Cell Sci.* **108**, 1239-1249.

Golomb, E., Ma, X., Jana, S. S., Preston, Y. A., Kawamoto, S., Shoham, N. G., Goldin, E., Conti, M. A., Sellers, J. R. and Adelstein, R. S. (2004). Identification and characterization of nonmuscle myosin II-C, a new member of the myosin II family. *J. Biol. Chem.* **279**, 2800-2808.

Holtzer, H., Croop, J., Dienstman, S., Ishikawa, H. and Somlyo, A. P. (1975). Effects of cytochaslasin B and colcemide on myogenic cultures. *Proc. Natl. Acad. Sci. USA* **72**, 513-517.

Kovacs, M., Wang, F., Hu, A., Zhang, Y. and Sellers, J. R. (2003). Functional divergence of human cytoplasmic myosin II: kinetic characterization of the non-muscle IIA isoform. *J. Biol. Chem.* **278**, 38132-38140.

Lo, C. M., Buxton, D. B., Chua, G. C., Dembo, M., Adelstein, R. S. and Wang, Y. L. (2004). Nonmuscle myosin IIb is involved in the guidance of fibroblast migration. *Mol. Biol. Cell* **15**, 982-989.

Maciver, S. K. (1996). Myosin II function in non-muscle cells. *BioEssays* **18**, 179-182.

Morgan, J. E., Beauchamp, J. R., Pagel, C. N., Peckham, M., Ataliotis, P., Jat, P. S., Noble, M. D., Farmer, K. and Partridge, T. A. (1994). Myogenic cell lines derived from transgenic mice carrying a thermolabile T antigen: a model system for the derivation of tissue-specific and mutation-specific cell lines. *Dev. Biol.* **162**, 486-498.

Musa, H., Orton, C., Morrison, E. E. and Peckham, M. (2003). Microtubule assembly in cultured myoblasts and myotubes following nocodazole induced microtubule depolymerisation. *J. Muscle Res. Cell Motil.* **24**, 301-308.

Peckham, M., Miller, G., Wells, C., Zicha, D. and Dunn, G. A. (2001). Specific changes to the mechanism of cell locomotion induced by overexpression of beta-actin. *J. Cell Sci.* **114**, 1367-1377.

Rosenfeld, S. S., Xing, J., Chen, L. Q. and Sweeney, H. L. (2003). Myosin IIb is unconventionally conventional. *J. Biol. Chem.* **278**, 27449-27455.

Sanger, J. W., Chowrashi, P., Shaner, N. C., Spalthoff, S., Wang, J., Freeman, N. L. and Sanger, J. M. (2002). Myofibrillogenesis in skeletal muscle cells. *Clin. Orthop. Relat. Res.* **403**, S153-S162.

Shewan, A. M., Maddugoda, M., Kraemer, A., Stehbens, S. J., Verma, S., Kovacs, E. M. and Yap, A. S. (2005). Myosin 2 is a key rho kinase target necessary for the local concentration of e-cadherin at cell-cell contacts. *Mol. Biol. Cell* **16**, 4531-4542.

Siebrands, C. C., Sanger, J. M. and Sanger, J. W. (2004). Myofibrillogenesis in skeletal muscle cells in the presence of taxol. *Cell Motil. Cytoskeleton* **58**, 39-52.

Swailes, N. T., Knight, P. J. and Peckham, M. (2004). Actin filament organization in aligned prefusion myoblasts. *J. Anat.* **205**, 381-391.

Takeda, K., Kishi, H., Ma, X., Yu, Z. X. and Adelstein, R. S. (2003). Ablation and mutation of nonmuscle myosin heavy chain II-B results in a defect in cardiac myocyte cytokinesis. *Circ. Res.* **93**, 330-337.

Tullio, A. N., Accili, D., Ferrans, V. J., Yu, Z. X., Takeda, K., Grinberg, A., Westphal, H., Preston, Y. A. and Adelstein, R. S. (1997). Nonmuscle myosin II-B is required for normal development of the mouse heart. *Proc. Natl. Acad. Sci. USA* **94**, 12407-12412.

Turney, S. G. and Bridgman, P. C. (2005). Laminin stimulates and guides axonal outgrowth via growth cone myosin II activity. *Nat. Neurosci.* **8**, 717-719.

Wang, F., Kovacs, M., Hu, A., Limouze, J., Harvey, E. V. and Sellers, J. R. (2003). Kinetic mechanism of non-muscle myosin IIB: functional adaptations for tension generation and maintenance. *J. Biol. Chem.* **278**, 27439-27448.

Wells, C., Coles, D., Entwistle, A. and Peckham, M. (1997). Myogenic cells express multiple myosin isoforms. *J. Muscle Res. Cell Motil.* **18**, 501-515.

Wylie, S. R. and Chantler, P. D. (2001). Separate but linked functions of conventional myosins modulate adhesion and neurite outgrowth. *Nat. Cell Biol.* **3**, 88-92.

Wylie, S. R. and Chantler, P. D. (2003). Myosin IIA drives neurite retraction. *Mol. Biol. Cell* **14**, 4654-4666.

Wylie, S. R., Wu, P. J., Patel, H. and Chantler, P. D. (1998). A conventional myosin motor drives neurite outgrowth. *Proc. Natl. Acad. Sci. USA* **95**, 12967-12972.